

ROW REMOVAL HEAT TRANSFER STUDY  
FOR PIN FIN ARRAYS

Kathryn L. Kirsch, Jason K. Ostanek\* and Karen A. Thole  
Pennsylvania State University  
Mechanical and Nuclear Engineering Department  
University Park, PA 16802

Eleanor Kaufman  
Pratt and Whitney  
400 Main Street  
East Hartford, CT 06108

ABSTRACT

Arrays of variably-spaced pin fins are used as a conventional means to conduct and convect heat from internal turbine surfaces. The most common pin shape for this purpose is a circular cylinder. Literature has shown that beyond the first few rows of pin fins, the heat transfer augmentation in the array levels off and slightly decreases. This paper provides experimental results from two studies seeking to understand the effects of gaps in pin spacing (row removals) and alternative pin geometries placed in these gaps. The alternative pin geometries included large cylindrical pins and oblong pins with different aspect ratios. Results from the row removal study at high Reynolds number showed that when rows four through eight were removed, the flow returned to a fully-developed channel flow in the gap between pin rows. When larger alternative geometries replaced the fourth row, heat transfer increased further downstream into the array.

INTRODUCTION

In the hot section of a gas turbine engine, gas path temperatures far surpass each component's melting temperature. Consequently, advanced cooling schemes are necessary to maintain the functional lifetime of the component and are integral in extending these lifetimes as engine designs progress. Cooling schemes are present on the exterior of components as well as in internal passages. Internal cooling can take numerous forms but in areas where structural support, in addition to high heat removal is necessary, pin fin arrays are commonly employed. Pin fins in this paper refer to pins that extend across the entire channel; note that many also refer to these features as pedestals. The addition of pin fins into the flow induces vortices at the pin base as well as increases the amount of surface area over which heat transfer can take place. The typical pin fin shape is a circular cylinder; much research has focused on the spacing variations of such pin fins and has reported on both row-averaged and overall array heat transfer. A consistent finding from these previous studies is that a peak

in heat transfer augmentation is seen near the third row of pins [1–4], depending on the streamwise spacing of the pins. Beyond this peak, a leveling off or even a slow decay in heat transfer augmentation is reported.

For these studies, a baseline configuration of sixteen rows of pin fins was studied at two different Reynolds numbers. This paper seeks to accomplish the following: understand changes in heat transfer when there is a gap in the pin fin array by removing a particular row; and understand the changes in augmentation when a row of alternatively-shaped pin fins is inserted into the gap.

NOMENCLATURE

$A_c$	pin cross sectional area
$A_{wet}$	wetted area
$D$	pin diameter
$D_h$	hydraulic diameter
$f$	Fanning friction factor
$f_0$	fully developed, smooth passage Fanning friction factor, $f_0 = (0.078)Re_{Dh}^{-0.25}$ [5]
$h$	heat transfer coefficient
$H$	pin fin height
$k$	air thermal conductivity
$k_p$	pin thermal conductivity
$L$	length of pin fin array, length of oblong pin
$m$	fin eigenvalue, $\sqrt{\left(\frac{hP}{k_p A_c}\right)}$ [6]
$N_{pins}$	number of pins in array
$N_{rows}$	number of pin rows
$Nu_{Dh}$	duct Nusselt number, $Nu_{Dh} = hD_h/k$
$Nu_0$	fully developed, smooth passage Nusselt number, $Nu_0 = 0.023Re_{Dh}^{0.8}Pr^{0.4}$ [7]
$p$	static pressure
$p_0$	static pressure in unobstructed duct
$P$	perimeter of pin
$q_{in}$	heat dissipated by foil heaters

\*Currently at the Naval Surface Warfare Center, Philadelphia, PA

$q_{\text{loss}}$	heat lost
$Re_D$	pin Reynolds number, $Re_D = U_{\text{max}} D v^{-1}$
$Re_{Dh}$	duct Reynolds number, $Re_{Dh} = U_m D_h v^{-1}$
$S$	spanwise spacing
$T$	temperature
$T_m$	mean channel temperature, or bulk temperature
$U_m$	mean channel velocity
$U_{\text{max}}$	maximum channel velocity
$W$	width of channel
$X$	streamwise spacing, streamwise position
$Y$	spanwise position

### Greek

$\Delta$	differential
$\varepsilon$	surface emissivity
$\rho$	air density
$\nu$	air kinematic viscosity
$\tau$	transmissivity of infrared viewing window

### PREVIOUS STUDIES

The general parameters of interest in investigating pin fin array heat transfer include varying spanwise ( $S$ ) and streamwise ( $X$ ) spacing, height-to-diameter ratio ( $H/D$ ) and Reynolds number. VanFossen and associates [3,4] provided early results on staggered pin fin arrays and reported on streamwise and spanwise spacings, as well as  $H/D$  variations. Lyall et al. [8] contributed results on the effects of spanwise spacing and Reynolds number variations on a single row of pin fins. Lawson et al. [9] added to the study done by Lyall et al. in analyzing the effects of both spanwise and streamwise spacing on a multi-row array of pin fins. The general trends found by these researchers were that decreased spacing in both spanwise and streamwise directions as well as increased Reynolds number led to higher array heat transfer. These conditions, however, also led to increased pressure drop in the channel.

Various correlations have also been developed to better predict heat transfer and pressure drop based on these key parameters of spacing, pin height and Reynolds number. Armstrong and Winstanley [10] provided a review on correlations previously developed for array-averaged heat transfer and array pressure drop. The authors applied these correlations to all existing data on pin fin heat transfer and were able to predict heat transfer to within 20% for  $H/D \leq 3$ ;  $1.5 \leq X/D \leq 5$ ; and  $2 \leq S/D \leq 4$ . [11] provided correlations taking into account  $H/D$  variations. The authors found that the Reynolds number exponent differed when  $H/D$  changed from 2 to 3. For  $H/D = 1$  and 2, the Reynolds number exponent was 0.65 and 0.75, respectively whereas when  $H/D = 3$  and 4, the Reynolds number exponent was 0.39 and 0.35, respectively. Recently Ostanek [12] provided correlations developed using artificial neural networks. His correlations were able to predict 73% of the available data on array-averaged heat transfer to within 10%.

Geometric considerations, apart from  $H/D$  variations, have also been studied. Engine-realistic pin fin fillets have been

examined by Chyu et al. [13], who found that such fillets decreased the overall heat transfer in the array as well as the pressure drop. Additionally, Arora and Abdel Messa [14] analyzed partial height pin fins, a potential by-product of manufacturing tolerances. The larger the gap between pin and endwall, the lower the heat transfer and corresponding pressure drop in the channel. Chyu et al. [15] also studied pins of different cross-sectional shape, such as squares and diamonds. The increased turbulence in the shear layers generated by these sharp-edged pins led to increased heat transfer. Tarchi et al. [16] examined cylindrical pins oriented in a pentagonal pattern in addition to staggered elliptical pins. Both studies were performed in a converging channel. The array of cylindrical pins generated similar heat transfer to a conventionally-spaced array, but with lower pressure drop. The elliptical pins, when oriented with their major axis perpendicular to the flow, generated higher heat transfer than a conventional pin fin array but seven times the pressure drop. Uzol and Camci [17] examined the heat transfer performance, generated turbulence and pressure drop across an array for elliptical pins as compared to circular cylindrical pins. Due to their streamlined shape and orientation in the channel, the elliptical pins generated far less turbulence in the channel than did the cylindrical pins. Consequently, their heat transfer performance was reduced.

In addition to overall average measurements, more detailed measurements are often required to gain further insights into pin fin heat transfer and the generated flowfield. Ames and associates [18–20] contributed detailed heat transfer, static pressure and turbulent intensity measurements to the field. In [20], Ames et al. provided correlations for local heat transfer coefficients based on local turbulence levels. A significant report was that the stagnation point heat transfer was most heavily influenced by the approach velocity. Ostanek and Thole [21, 22] characterized the effect of Reynolds number and spacing on the flowfield in a pin fin array. Increasing Reynolds number led to shorter near wakes that correlated with higher heat transfer. In [22], the authors showed that streamwise spacings closer than 2.16 pin diameters suppressed the typical vortex shedding pattern seen behind pin fins in cross flow. Also important to note is that due to the proximity of the pins, a typical turbulence decay such as that downstream of a bar grid does not apply.

One well-known behavior of heat transfer through pin fin arrays is that the heat transfer augmentation initially increases when it hits the first row of pins, reaches a peak near the third row of pins and then decreases gradually through the remainder of the array. Many researchers have sought alternative solutions to this issue. Busche et al. [23] replenished the coolant fluid periodically through a multi-row array, thereby reinitializing the heat transfer capacity of the fluid. Local increases in heat transfer were indeed seen where the coolant was replenished. Ostanek and Thole [24] examined non-uniform streamwise spacing: streamwise spacing was widest at the front of the array and steadily decreased toward the back of

the array. A constant closely-spaced array outperformed the non-uniformly spaced array.

Metzger et al. [1] studied the effects of removing rows in the middle of an array in order to create a disruption in the flow. Four rows were sequentially removed, starting in the fourth row. Row-averaged results showed that for all cases, heat transfer beyond the gap in pins recovered to the same magnitude; the global peak in heat transfer was still seen in the third row. Metzger et al. [1] also experimented with two different diameter pin fin shapes. The authors inserted three rows of large diameter pin fins ( $H/D = 0.6$ ) behind three rows of their conventional pin,  $H/D = 1$ . The change in  $H/D$  ratio disrupted the flow such that a significant increase in heat transfer was seen where the larger diameter pin fins began.

This review of relevant literature shows that a large focus in pin fin studies is on retaining high heat transfer performance throughout an entire array. While Metzger et al. [1] performed a row removal study, detailed measurements on the heat transfer throughout the channel were not presented. Such details are one part of the focus for this paper in addition to the effects of Reynolds number on these row removal experiments. Similarly, while Metzger et al. [1] also studied the combination of pins with two different  $H/D$  ratios, the study was performed for only six rows of pins and did not include any other alternative shapes. The present study seeks to understand the heat transfer and pressure drop effects of combining alternatively shaped pins, including two oblong shapes, with cylindrical pins. Additionally, this study also includes one experiment containing cylindrical pins with two different  $H/D$  ratios.

## EXPERIMENTAL FACILITY

All experiments were performed in a recirculating channel and all data were taken under steady conditions. Figure 1 shows a schematic of the test facility, which has been previously used for experiments in [8, 9, 24], among others. Room temperature air was driven through the test section using a centrifugal blower controlled by an electric motor capable of  $0.66 \text{ m}^3/\text{s}$ . Flow exited the blower and first traveled through a Venturi meter used to measure the mass flow rate through the test section. The flow then entered the inlet plenum, where splash plates were located to prevent jet formation in the channel. Also in the inlet plenum was a heat exchanger used to remove excess heat created by the blower as well as from the heaters in the test section. Flow entered the test section through a rounded edge contraction and passed over coarse grit sandpaper to encourage turbulent flow. The flow passed through a distance of  $37D_h$  before reaching the edge of the heaters and another  $5D_h$  before reaching the first row of pins. The height of the channel was  $8.9 \text{ mm}$  ( $0.51D_h$ ), the width  $0.51 \text{ m}$  ( $29D_h$ ) and the length  $1.65 \text{ m}$  ( $94D_h$ ). Beyond the test section was an exit plenum that also contained a splash plate; through the exit plenum, the flow reentered the blower.

Experiments in this test facility were conducted at two duct Reynolds numbers of  $5.0e3$  and  $2.0e4$  while the pin

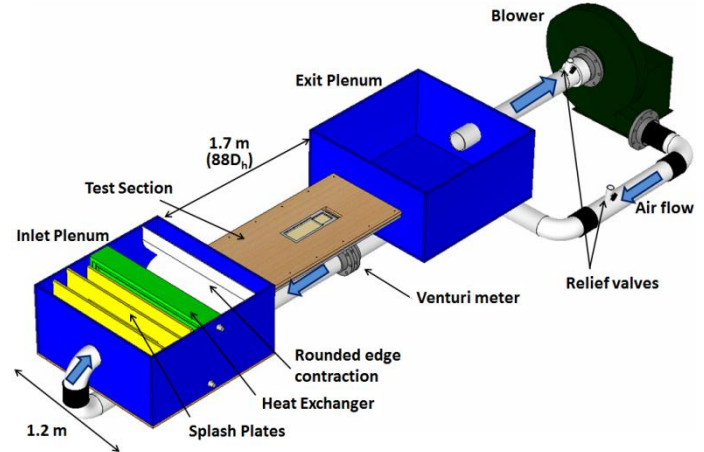


Figure 1. Schematic of the test facility used for all experiments [24].

Reynolds numbers were  $5.3e3$  and  $2.1e4$ , respectively. The parameters used in the calculation of duct Reynolds numbers were the mean channel velocity and the hydraulic duct diameter. In the calculation of the pin Reynolds number, the maximum velocity through the channel (occurring through the minimum flow area) and the pin diameter were used.

The baseline test contained 16 rows of cylindrical pins at a constant spanwise and streamwise spacing of  $2.33$  pin diameters. In the cases where rows four through eight were sequentially removed, the remaining pins were kept at the same constant spacing. Similarly, where rows four and five were replaced with one row of alternatively-shaped pins, all cylindrical pins were kept at the constant spacing of the initial study. The spacing of the alternatively-shaped pins varied depending on their geometry. Table 1 shows the spacings and geometries of the baseline and alternative geometry tests. Each pin was constructed from copper and exhibited high pin efficiencies, where pin efficiency was calculated using equation 1. The efficiency of the baseline pin was  $99.8\%$ . The  $\pm 30^\circ$  oblong pin, large diameter pin fin and large oblong pin had efficiencies all over  $99\%$ . Equation 1 assumes an adiabatic fin tip; the length used was therefore half the pin height.

$$\eta = \frac{\tanh\left[m\left(\frac{H}{2}\right)\right]}{m\left(\frac{H}{2}\right)} \quad 1)$$

The channel endwalls were constructed from medium density fiberboard (MDF) with a low thermal conductivity of  $k = 0.124 \text{ W/m}\cdot\text{K}$ . A window was cut into the top endwall in order that the infrared (IR) camera had access to the heated test section. The heat transfer results from these studies included the contributions from the both the pin surface and endwall, as both surfaces were heated. The copper pins were adhered to the heaters using a thermally conductive and electrically insulating epoxy ( $k = 4 \text{ W/m}\cdot\text{K}$ ). The heaters provided a constant heat flux boundary condition. The bottom heater was a commercially available Kapton serpentine heater whereas the

top heater was a custom-made Inconel foil heater covered in Kapton tape to ensure electrical insulation. The thin, smooth foil allowed for detailed heat transfer features to be captured by the IR camera, which measured temperatures by viewing the non-flow side of the Inconel foil lining the top endwall. The commercially-available Kapton heater was durable and was left in place for many experiments before needing replacement.

The custom-made Inconel foil heater was less durable. The center strip of Inconel, which covered the aforementioned IR-viewing window cutout on the top endwall, was largely unsupported. This strip was replaced for each experiment. The two side Inconel strips were fully adhered to the endwall and were therefore able to withstand multiple tear-downs and rebuilds. The three strips of Inconel were connected in series via copper bus bars.

**Table 1. Dimensions and Orientations of Pin Fin Arrays**

Pin	H/D	L/D	Orientation
Baseline 16-row geometry	0.8	N/A	
$\pm 30^\circ$ Oblong	0.8	3	
Large diameter pin fin	0.47	N/A	
Large oblong	0.47	2.5	

The flow was validated to be fully developed through both heat transfer and friction factor tests with an unobstructed duct. Results were within the experimental uncertainty for published literature on empty duct flows. The validation for hydrodynamically fully developed flow was described in more detail in previous studies [9]. For every test, the empty duct Nusselt number was checked against the Dittus-Bolter correlation and matched to within experimental uncertainty, thus confirming thermally fully-developed flow. Uncertainty will be discussed in a later section.

### MEASUREMENT TECHNIQUE

As previously mentioned, the top endwall contained a cutout through which the IR camera had viewing access to the heated pin fin array, as shown in Figure 2. Atop this window cutout was placed a Zinc-Selenide (ZnSe) window that provided high transmissivity ( $\tau = 0.7$ ) in the IR spectrum as well as a form of thermal insulation. The IR camera, therefore, measured temperatures by viewing the non-flow side of the Inconel heater through the ZnSe window, which sat in the top endwall cutout. The thickness of the air gap between the ZnSe window and the non-flow side of the Inconel heater (6.35 mm) was chosen such that the conduction losses through the top and bottom heaters were of similar magnitude. Silicone sealant was placed around the edges of the cutout window to ensure a tight seal between heater and endwall; the cutout window sides and heater were then spray-painted black to give high emissivity ( $\epsilon = 0.93$ ).

The images taken by the IR camera were analyzed for the heat transfer coefficient at each pixel. Each IR image was calibrated using thermocouples adhered to the heater surface by the same thermally conductive epoxy used between the pins and heaters. As the results of interest were the combined pin and endwall surface contributions to heat transfer, each pixel, regardless of its location relative to a pin, was analyzed in the same manner. Equation 2 shows the general equation for obtaining the heat transfer coefficient at each pixel location.

$$h(x,y) = \frac{q_{in} - \sum q_{loss}(x,y)}{A_{wet}(T(x,y) - T_m(x,y))} \quad 2)$$

The heat flux into the system was a known quantity and set for each experiment. The losses represented a combination of the radiative losses through the endwall cutout as well as conductive losses through both sides of the test section. The local wall temperature reading was given from the IR camera and the local bulk temperature was calculated from the first law

knowing the net heat added into the flow and inlet gas temperature. The wetted area is given by equation 3.

$$A_{\text{wet}} = 2N_{\text{rows}}XW + N_{\text{pins}}\left(\pi DH - \frac{\pi D^2}{2}\right) \quad (3)$$

The first term in equation 3 represented the array area, which included one half pitch upstream of the first row of pins and one half pitch downstream of the last row of pins. To that value, the surface area of the pins was added and next the footprint area of the pins was subtracted. As both endwall surfaces were included in the calculation, two pin footprints were subtracted in Equation 3. Note that as pin rows are removed, the wetted area changed appropriately.

Figure 2 shows a cutout view of the test section and highlights the test section features. Insulation was placed around the entirety of the test section to minimize losses. Conduction losses through the channel were measured with pairs of thermocouples mounted on the bottom endwall. One set of thermocouples was placed beneath the bottom heater and the other on the far side of the endwall, directly atop the insulation. Conduction losses were assumed to be symmetric. As previously mentioned, the air gap width between the ZnSe window and the top endwall was chosen such that conduction losses through the top and bottom endwalls were similar. Given that the difference between the two measured conduction losses reached only 5% at the worst case scenario, the assumption of symmetry was deemed acceptable. Radiation losses were calculated only through the endwall cutout and were calculated to be 4% of the total heat flux. Properly accounting for the heat losses was confirmed through the comparison of the Nusselt number upstream of the pins (empty duct) to the Dittus-Boelter correlation. As previously mentioned, each experiment showed an agreement within the experiment uncertainty. A detailed description of the heat loss calculations can be found in [25].

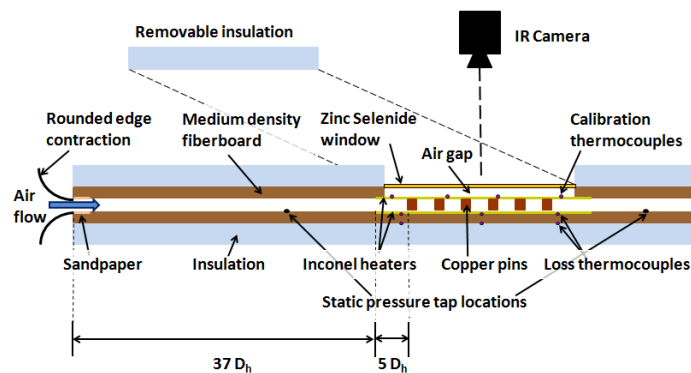


Figure 2. Cutout view of the test section.

In addition to heat transfer data, the pressure drop across the array, presented as a friction factor, was recorded. Five pairs of static pressure taps were mounted on the test section, where one set of taps was located upstream of the array and the other set located downstream. An average of the five measured

pressure drops was taken and used in the equation for the Darcy friction factor, shown in equation 4.

$$f = \left(\frac{\Delta p - \Delta p_0}{0.5\rho U_m^2}\right)\left(\frac{D_h}{L}\right) \quad (4)$$

The term  $\Delta p_0$  was the pressure drop across the empty duct, which was calculated from  $f_0$ , the empty duct friction factor. The equation for  $\Delta p_0$  is given in equation 5.

$$\Delta p_0 = f_0(2\rho U_m^2)\left(\frac{L - (N + 1)X}{D_h}\right) \quad (5)$$

To note, the Mach number in all parts of the channel was less than 0.1 and therefore, the friction factor measurements for all tests were for incompressible flow.

## UNCERTAINTY ANALYSIS

Measurement uncertainty was calculated using the sequential perturbation method, as described by Moffat [26]. Uncertainty was calculated at a 95% confidence level. The maximum uncertainty in Reynolds number was 1.5%. Nusselt number uncertainty for low Reynolds number was calculated at 11.1% and for high Reynolds number was calculated to be 6.7%. The uncertainty in heat transfer was due to the measured heat flux, heater surface temperature and the bulk flow measurement. The friction factor uncertainty was calculated at 10.0% at the low Reynolds number and 9.6% at the high Reynolds number. The uncertainty in friction factor was driven by the pressure transducers used to measure the extremely small pressure drop across the pin fin array.

## RESULTS AND DISCUSSION

The forthcoming results present the insights gained from two modifications to a baseline study of pin fin heat transfer as was previously discussed. The baseline study contained sixteen rows of cylindrical pin fins, spaced at  $X/D = S/D = 2.33$ , and results were analyzed for two duct Reynolds numbers of  $5.0e3$  and  $2.0e4$ .

### Row Removal Studies

Experiments performed while sequentially removing middle rows from a pin fin array answered two questions. The first was whether and at what distance the flow returned to being fully developed after traveling through three rows of pins. The second was whether a second peak in heat transfer, comparable to that seen in the third row of pins, would occur after the flow had been returned to its fully developed state.

Figure 3 shows heat transfer augmentation contours for each of the row removal studies at the low Reynolds number of  $5.0e3$ . Heat transfer augmentation was measured relative to an empty duct Nusselt number, calculated by the Dittus-Bolter correlation [7]. The center of the first row of pins was located at  $X/D = 0$ . As a confirmation of thermally fully developed flow upstream of the pins, the augmentation in this area was

near unity. The agreement among all six tests in the first three rows of pins was within the experimental uncertainty.

Figure 3 shows that at the low Reynolds number of  $5.0e3$ ,

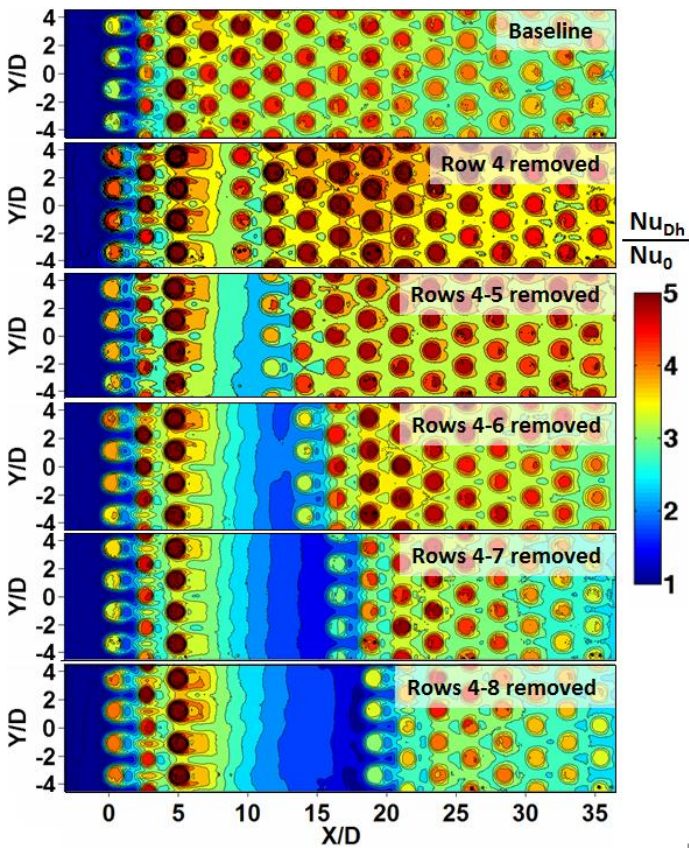


Figure 3. Heat transfer augmentation contours for the row removal studies at  $Re_{Dh} = 5.0e3$ .

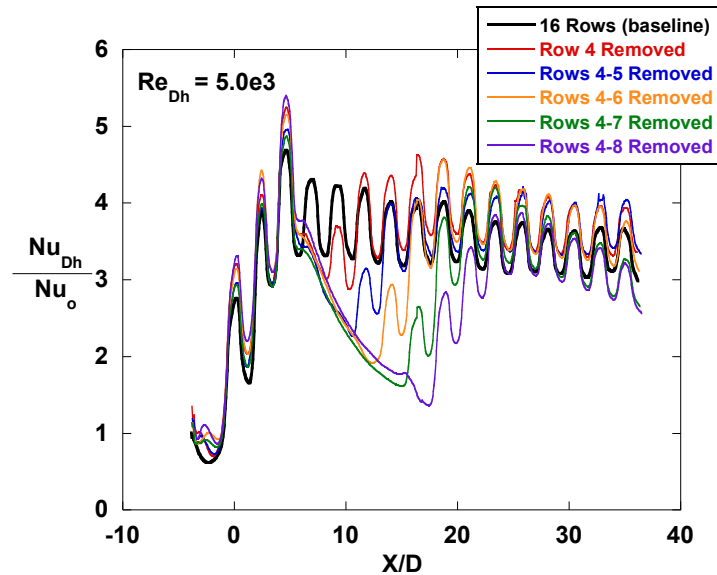


Figure 4. Laterally averaged heat transfer augmentation for the row removal studies at  $Re_{Dh} = 5.0e3$ .

the flow did not return to a fully developed state in the gap between pins. The low momentum provided by such a low Reynolds number was not enough to fully dissipate the vortical structures generated by the pins. With such weak vortical structures, the fully developed channel flow was not reestablished. Therefore, even in the cases with rows 4-7 and 4-8 removed, where the flow appeared to be nearly fully developed, high peaks in heat transfer through the reinstated pins were not seen. The augmentation contours also showed where the wakes were still mixed out corresponded to where the fluid's heat transfer capacity was still diminished.

Figure 4 shows laterally averaged heat transfer augmentation versus streamwise distance,  $X/D$  for the low Reynolds number case. These datasets validated the observations made from the augmentation contours in Figure 3 and highlighted some of the flow phenomena. The local peaks in heat transfer were the locations of the pins; the global peak was seen at the third row of pins. Indeed, the augmentation in the gap never reached unity; its lowest value was  $Nu_{Dh}/Nu_0 = 1.5$ . When row 4 was removed, the peak from the second row of reinstated pins was higher than the peak from the baseline study at that point. Further, the peaks from the row 4 removed study continued to surpass the peaks from the baseline study downstream into the array. As a point of contrast, in the case where rows 4-8 were removed, the peaks in heat transfer did

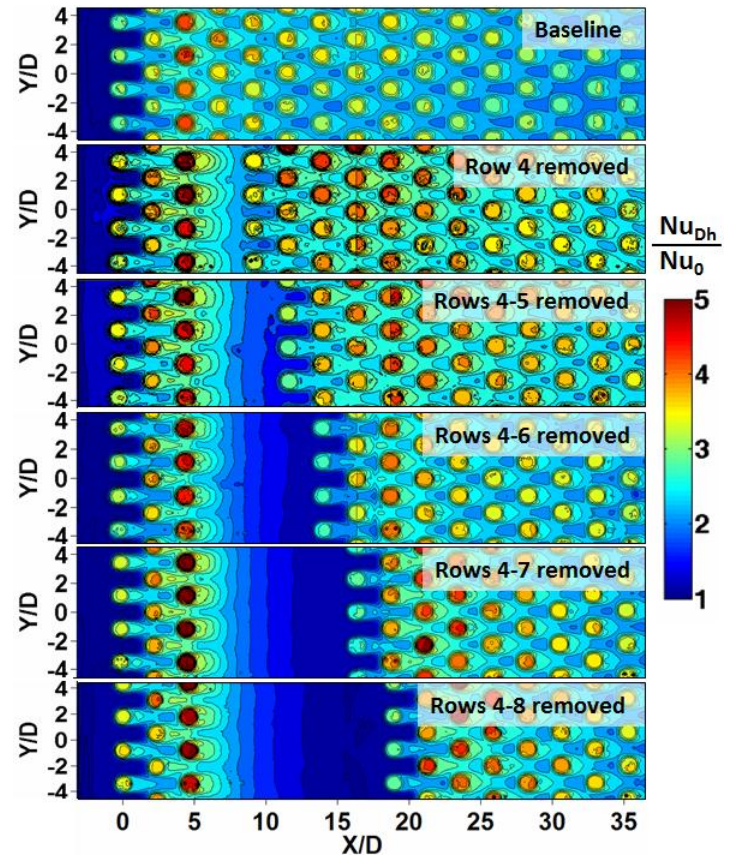


Figure 5. Heat transfer augmentation contours for the row removal studies at  $Re_{Dh} = 2.0e4$ .

not surpass those of the baseline at any point in the array. At the back of the array, the baseline study even outperformed the study with rows 4-8 removed as well as the study with rows 4-7 removed. With the exception of the case with rows 4-8 removed, all tests showed a recovery to the baseline case in the second reinstalled row. When rows 4-8 were removed, recovery to the baseline study was seen by the third row of reinstalled pins.

At the high Reynolds number of  $2.0 \times 10^4$ , the decay to fully developed flow occurred earlier in the array, as seen in Figure 5. The higher turbulent flow led to the dissipation of the vortices and the flow did in fact return to a fully developed state when rows 4-8 were removed. The behavior of the flow in the first few rows of reinstalled pins in the cases of rows 4-7 and 4-8 removed mimicked the behavior of the first three rows in the array.

Figure 6 shows the laterally averaged heat transfer augmentation for the high Reynolds number. As was seen in Figure 5, the augmentation was near unity in the case of rows 4-8 removed. The decay length to an augmentation of one was approximately 8 hydraulic diameters. Experiments with rows 4, 4-5 and 4-6 removed showed a recovery to the baseline study after the second row of reinstalled pins, which was the behavior seen at the low Reynolds number. However, tests with rows 4-7 and 4-8 recovered to the baseline study before the peak at the second row of reinstalled pins.

A particular result of note was that the datasets from rows 4-6, 4-7 and 4-8 removed all showed that the first rows of pins after the gap had peaks of the same magnitude. The peaks behind the reinstallation of pins, however, differed indicating that the number of rows removed influenced the extent of the impact on downstream heat transfer. An incoming flow with augmentation greater than one has not fully recovered its heat transfer capacity, as was the case with rows 4-6 removed. With rows 4-7 removed, the peak near  $X/D = 22$  (three rows behind

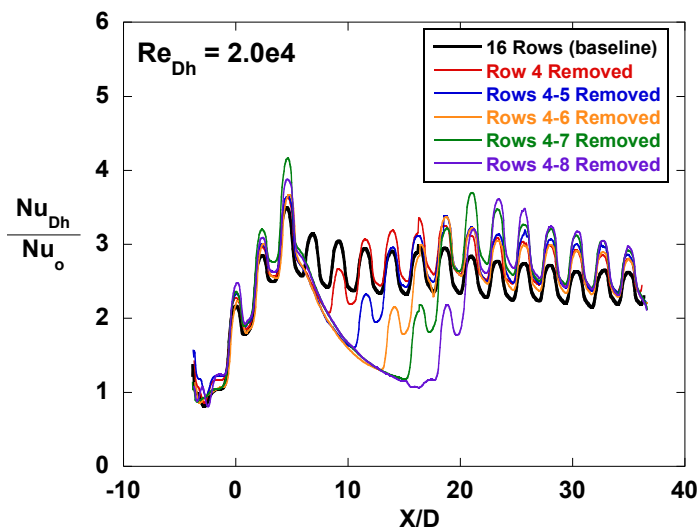


Figure 6. Laterally averaged heat transfer augmentation for the row removal studies at  $Re_{Dh} = 2.0 \times 10^4$ .

the reinstallation of pin fins) nearly reached the average peak seen near  $X/D = 5$  (row 3). Similarly, with rows 4-8 removed, the peak near  $X/D = 24$  was significantly above the peaks at that location from the other tests. Also to note was the magnitude of all peaks beyond  $X/D = 20$ . The baseline study showed the smallest peaks in this region. Such behavior indicated that even if the flow had not returned to a fully developed flow in the gap, the mere presence of the gap worked to reset the decay in heat transfer.

### Alternative Pin Geometries

As previously mentioned, the second study of interest in understanding pin fin heat transfer included inserting one row of alternatively-shaped pins in the place of two rows of cylindrical pins. Rows 4-5 were removed from the baseline study so that the performance of the alternatively shaped pins could be evaluated. The alternatively shaped pins included two oblong shapes and one large diameter circular cylinder, the dimensions and orientations of which were given in Table 1. Like in the row removal studies, each experiment was run at a low and high duct Reynolds number of  $5.0 \times 10^3$  and  $2.0 \times 10^4$ , respectively.

Figure 7 shows the heat transfer augmentation contours for the alternative geometry study at the low Reynolds number. In addition to the experiments with combined conventional and alternatively-shaped pin fins, the baseline study and the row removal study with rows 4-5 removed were shown for comparison. The sizes of the images containing alternative geometries were chosen such that the array was periodic over the top and bottom edges. One result of note was the

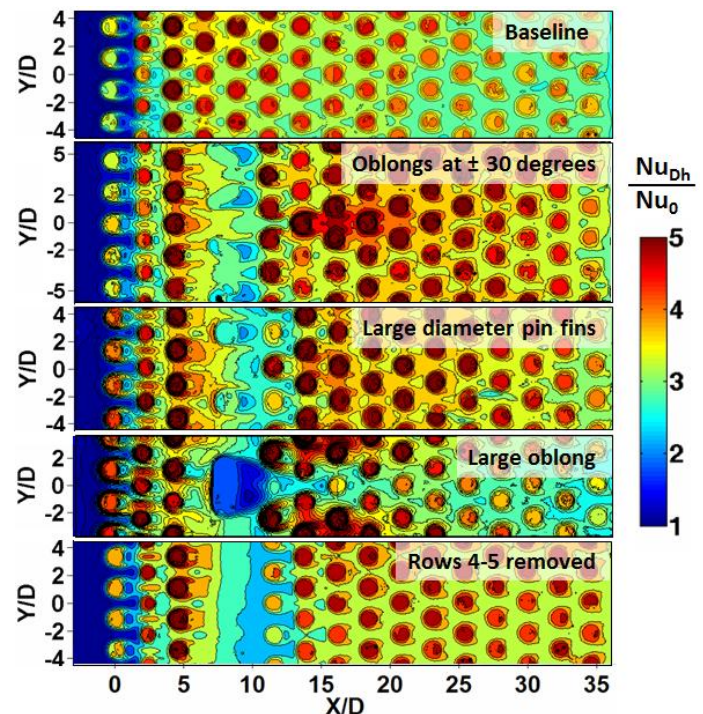


Figure 7. Heat transfer augmentation contours for the alternative geometry studies at  $Re_{Dh} = 5.0 \times 10^3$ .

performance of the alternatively-shaped pins themselves. In all cases, the heat transfer augmentation in the region containing the alternative geometry was well below that of the baseline study. However, all three alternative geometries imposed an obvious change in flow direction. The  $\pm 30$  degree oblongs channeled the flow between them, creating a diamond shape of high heat transfer augmentation beginning two rows behind them. Similarly, the large diameter pin fins prevented the pins immediately behind them from exhibiting high heat transfer augmentation; where a conventional-sized pin was located in between the large diameter pins was an area of higher local heat transfer. Lastly, the large oblong produced two diamond-shaped regions of high heat transfer. Directly behind the large oblong pin, the heat transfer was low because of the lack of flow seen by these pins. The large oblong created the longest-lasting effect on the heat transfer from the array.

Figure 8 shows the laterally averaged heat transfer augmentation for the contours shown in Figure 7. In looking at  $6 \leq X/D \leq 11$ , where the alternative geometries were placed, the decay of heat transfer augmentation was similar to the row removal studies. However, beyond  $X/D = 11$ , or where the rows of conventional pin fins were reinstated, significant differences between the two types of studies were seen. In the experiment with the large oblong, heat transfer augmentation recovered quickly and to a magnitude that reached the augmentation seen in the third row of pins. The long-lasting negative effects of the large oblong, however, were seen clearly in the laterally averaged plot beyond  $X/D = 25$ . The oblongs oriented at  $\pm 30^\circ$  and the large diameter pin fins also recovered their heat transfer augmentation faster than the row removal study and showed similar results. These two studies showed increased augmentation over the baseline study over the remaining length of the array,  $15 \leq X/D \leq 35$ .

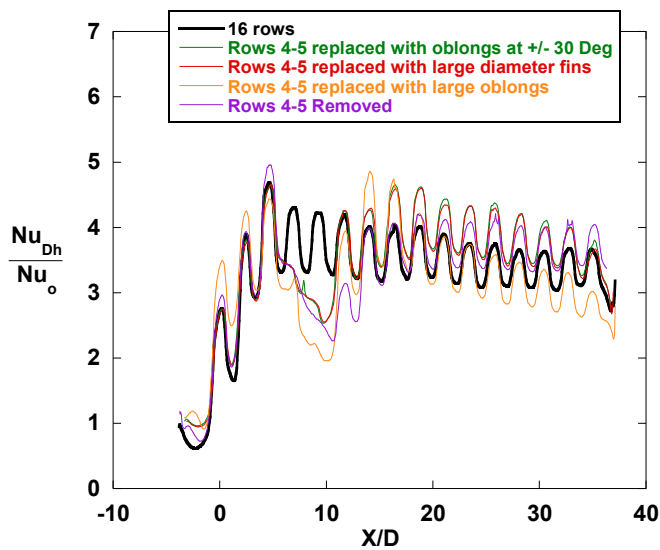


Figure 8. Laterally averaged heat transfer augmentation for the alternative geometry studies at  $Re_{Dh} = 5.0e3$ .

Figure 9 shows the augmentation contours for the alternative geometry studies at the high Reynolds number of  $2.0e4$ . Again, the sizes of the contours were picked such that the results were symmetric across the top and bottom boundaries. The trends seen at the low Reynolds number were repeated at the high Reynolds number, though with decreased peaks in heat transfer. Where conventional pins were directly behind an alternatively-shaped pin, the heat transfer augmentation was low; where the flow was redirected and consequently accelerated, heat transfer augmentation was high.

Figure 10 shows the laterally averaged heat transfer augmentation for the contours seen in Figure 9. As was seen in the augmentation contours, the laterally averaged plot showed higher heat transfer from the baseline study than from each of the alternative geometries in the fourth and fifth rows. However, one difference in this area was the performance of the oblongs at  $\pm 30^\circ$ ; their decay in heat transfer no longer matched the three other experiments. Also, the heat transfer recovery of the  $\pm 30^\circ$  oblongs was the quickest and the peak in the first row of reinstated pins was the highest at that point. In the second and third rows of reinstated pins, the heat transfer for each of the alternative geometries showed improvements over the baseline study. However, with increasing distance into the array, the heat transfer levels of the alternative geometries decreased to the levels seen by the baseline study. At the higher Reynolds number, the higher momentum flow mixed out the effect of the alternative geometries quicker than in the low Reynolds number tests. The spread in heat transfer augmentation at the back of the array was small.

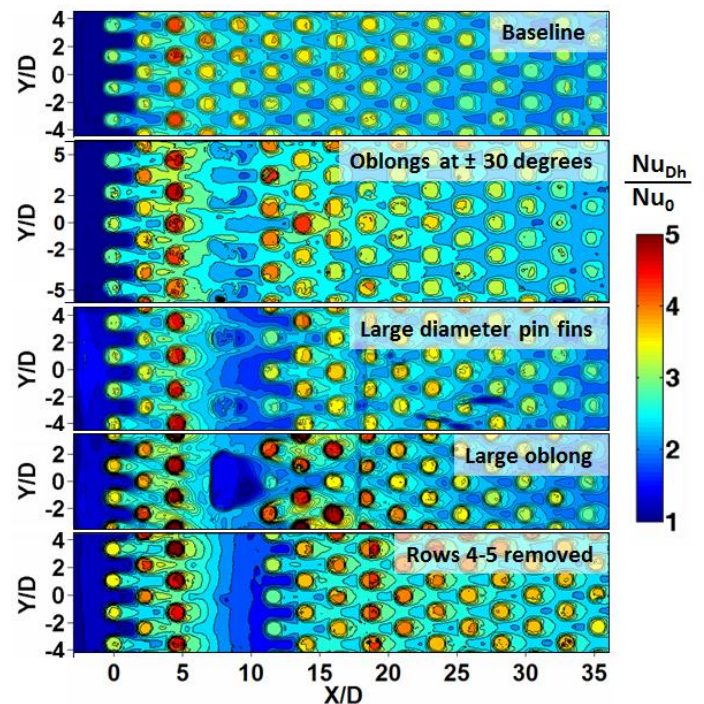


Figure 9. Heat transfer augmentation contours for the alternative geometry studies at  $Re_{Dh} = 2.0e4$ .

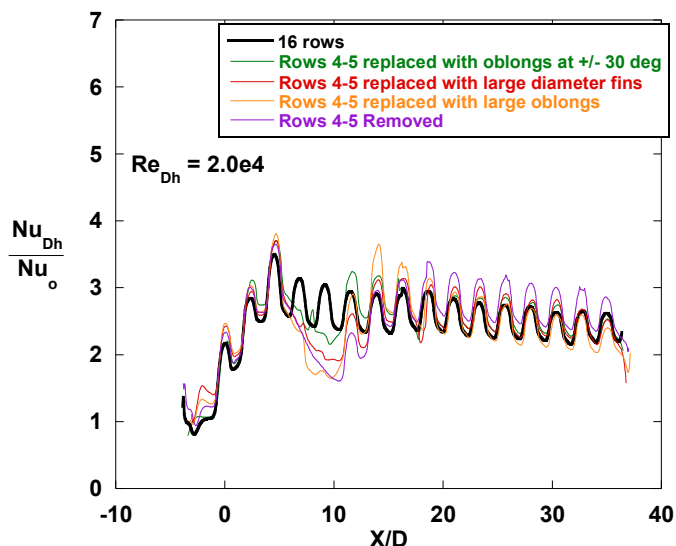


Figure 10. Laterally averaged heat transfer augmentation for the alternative geometry studies at  $Re_{Dh} = 2.0e4$ .

### Pressure Loss Measurements

For both the row removal and alternative geometry studies, the pressure drop across the array was measured and converted to a friction factor. Five sets of pressure taps were mounted flush with the test section, with one set located upstream of the array and the other located downstream of the array. The average of the five pressure drop readings were used in the calculation of the friction factor.

Figure 11 shows the friction factor versus array-averaged heat transfer. For comparison, the empty duct friction factor,  $f_0$ , was plotted against the Dittus Bolter correlation for heat transfer,  $Nu_{Dh}$ . The two clusters of data represent the two Reynolds numbers studied. For both Reynolds numbers, the highest friction factor was seen for the baseline study, though the spread was minimal at the highest Reynolds number. In each of the other experiments, the density of pins was always less than the density of baseline study. Therefore, each of these other tests showed slightly lower friction factor than the baseline study. The steady decrease in both heat transfer and friction factor for the row removal studies was to be expected. The higher Reynolds number appeared to influence this decrease in heat transfer and friction factor more strongly.

In looking at the alternative geometry tests and the baseline study, the friction factors for all four tests were within 25% of each other. From this information, a conclusion could be drawn that the friction factor is heavily dominated by the cylindrical pins.

Another point of interest was the array averaged heat transfer for each of the alternative geometry tests. The data were again clustered with respect to the y-axis, indicating that the alternative geometries do not significantly influence the overall heat transfer performance. As previously pointed out, the advantages and disadvantages of the alternative geometries are better analyzed in looking at the detailed localized results.

Figure 12 shows friction factor augmentation versus array averaged heat transfer augmentation. Like in Figure 11, the two clusters of data represent the two Reynolds numbers studied. Much like the trend seen in Figure 11, the row removal studies showed decreasing friction factor augmentation and heat transfer augmentation with more rows removed at both Reynolds numbers. At the low Reynolds number, the data showed a trend in heat transfer augmentation where a slight peak was seen at the  $\pm 30$  degree oblongs. However, at the higher Reynolds number, the trend in heat transfer augmentation and friction factor augmentation was a relative steady increase in both values.

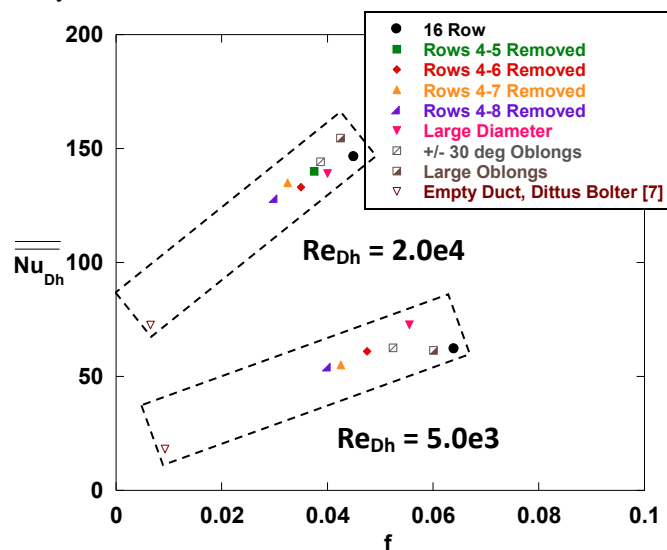


Figure 11. Effect of alternative geometries on friction factor and array averaged heat transfer at both Reynolds numbers.

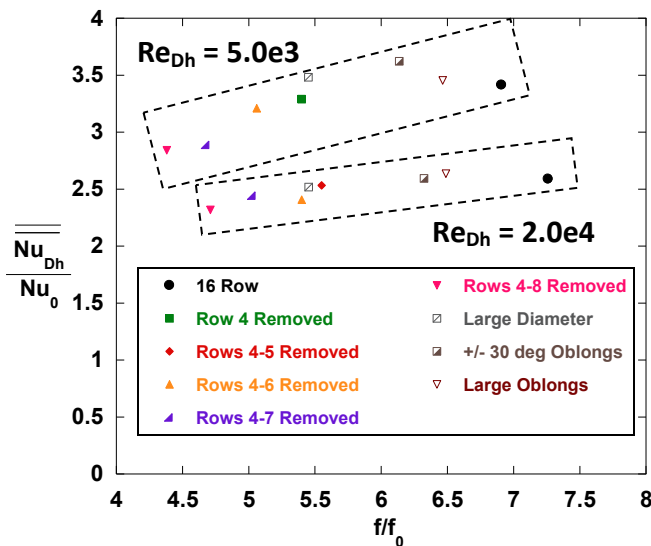


Figure 12. Friction factor augmentation vs. heat transfer augmentation at both Reynolds numbers.

## CONCLUSIONS

Two modifications to a baseline multi-row pin fin array were performed to gain insights into the heat transfer capabilities of such arrays. First, beginning in the fourth row of the baseline study, five rows were sequentially removed and heat transfer and pressure loss measurements were conducted for two Reynolds numbers of  $5.0 \times 10^3$  and  $2.0 \times 10^4$ . Second, one row of alternatively shaped pins was inserted into the space previously taken by two rows of conventional pins. Three different geometries were used for these experiments and included one large diameter cylindrical pin and two oblong pins of different dimensions. Again, heat transfer measurements were taken, as well as pressure drop measurements for two Reynolds numbers of  $5.0 \times 10^3$  and  $2.0 \times 10^4$ .

For the low Reynolds number case of the row removal study, the flow never returned to a fully developed flow in the region where pins were removed. The momentum from the flow was not enough to fully dissipate the vortical structures in the channel. Therefore, the heat transfer pattern through the first few rows of reinstalled pins never matched the desirable pattern seen in the first three rows of the array. At the high Reynolds number, however, the flow was able to return to fully developed in the empty space in the array. Consequently, peaks in heat transfer behind the gap in pin fins were reminiscent of those seen in the first three rows of an array. To note, however, the global peak in heat transfer was still always found in the third row of pins.

In the case of the alternative geometry experiments, all three alternatively-shaped pins created significant differences in flow patterns at both Reynolds numbers. Such large obstructions redirected the flow in the channel; pins that were located directly behind the larger obstructions showed much reduced heat transfer augmentation. Conversely, pins in the path of the redirected, accelerated flow showed local enhancements in heat transfer further downstream from the obstruction. To note, each of the obstructions themselves showed poor heat transfer augmentation. Their benefit came locally in the redirected flow 1-3 rows downstream.

The pressure drop through the baseline geometry and the arrays containing alternative geometries was similar among all cases, at both Reynolds numbers. Expectedly, the row removal studies showed correspondingly lower heat transfer and friction factor values as more rows were removed. The friction factor was largely dominated by the number of conventional pins in the array; one row of alternatively-shaped pins had a small effect on the pressure drop. Similarly, the overall heat transfer performance of the arrays was clustered together at each of the Reynolds numbers. The benefits from the alternative geometries were local and when an array average was taken, such benefits were marginalized by the disadvantages of having such a large obstruction in the array.

These results contribute to the knowledge on pin fin array heat transfer through detailed studies on the middle rows of an array. Local changes to the array indeed create local changes to the heat transfer, but largely do not affect the overall heat

transfer or pressure drop to an array. This information is useful for designs where such local effects may be desired. Additionally, these studies can help predict the combined effects of different pin fin shapes on the heat transfer through the array.

## ACKNOWLEDGMENTS

The authors would like to acknowledge Pratt and Whitney and the Department of Defense Science, Math and Research for Transformation (SMART) fellowship program for sponsoring this work.

## REFERENCES

- [1] Metzger D. E., Shepard W. B., and Haley S. W., 1986, "Row Resolved Heat Transfer Variations in Pin-Fin Arrays Including Effects of Non-Uniform Arrays and Flow Convergence," ASME Paper No. 86-GT-132.
- [2] Metzger D. E., Fan Z. X., and Shepard W. B., 1982, "Pressure Loss and Heat Transfer through Multiple Rows of Short Pin Fins," Heat Transfer 1982, Proceedings of the 7th International Heat Transfer Conference. Volume 6: General Papers: Combined Heat and Mass Transfer, Particle Heat Transfer, Heat Exchangers, Industrial Heat Transfer, Heat Transfer in Energy Utilization., Hemisphere Publ Corp, pp. 137–142.
- [3] VanFossen G. J., 1982, "Heat Transfer Coefficients for Staggered Arrays of Short Pin Fins," ASME Paper No. 81-GT-75.
- [4] Simoneau R. J., and VanFossen G. J., 1984, "Effect of location in an array on heat transfer to a short cylinder in crossflow," J. Heat Transf., **106**(1), pp. 42–48.
- [5] Colebrook C. F., 1939, "Turbulent flow in pipes, with particular reference to the transition region between the smooth and rough pipe laws," J. Inst. Civ. Eng., pp. 133–156.
- [6] Incropera F. P., and Dewitt D. P., 2002, Fundamentals of Heat and Mass Transfer, New York, New York.
- [7] McAdams W. H., 1942, Heat Transmission, McGraw-Hill Book Company, Inc, New York, New York.
- [8] Lyall M. E., Thrift A. A., Thole K. A., and Kohli A., 2011, "Heat transfer from low aspect ratio pin fins," J. Turbomach., **133**(1).
- [9] Lawson S. A., Thrift A. A., Thole K. A., and Kohli A., 2011, "Heat transfer from Multiple Row Arrays of Low Aspect Ratio Pin Fins," Int. J. Heat Mass Transf., **54**(17-18), pp. 4099–4109.
- [10] Armstrong J., and Winstanley D., 1988, "A Review of Staggered Array Pin Fin Heat Transfer for Turbine Cooling Applications," J. Turbomach., **110**(1), p. 94.
- [11] Chyu M. K., Siw S. C., and Moon H. K., 2009, "Effects of height-to-diameter ratio of pin element on heat transfer from staggered pin-fin arrays," 2009 ASME Turbo Expo, June 8, 2009 - June 12, 2009, American Society of Mechanical Engineers, pp. 705–713.
- [12] Ostanek J. K., 2013, "Improving Pin-Fin Heat Transfer

- Predictions using Artificial Neural Networks,” *J Turbomach.*
- [13] Chyu M. K., 1990, “Heat Transfer and Pressure Drop for Short Pin-Fin Arrays with Pin-Endwall Fillet,” *Trans. ASME J. Heat Transf.*, **112**(4), pp. 926–32.
- [14] Arora S. C., and Abdel-Messeh W., 1990, “Characteristics of Partial Length Circular Pin Fins as Heat Transfer Augmentors for Airfoil Internal Cooling Passages,” *J. Turbomach.*, **112**(3), pp. 559–565.
- [15] Chyu M. K., Hsing Y. C., and Natarajan V., 1998, “Convective Heat Transfer of Cubic Fin Arrays in a Narrow Channel,” *J. Turbomach.*, **120**(2), pp. 363–367.
- [16] Tarchi L., Facchini B., and Zecchi S., 2008, “Experimental Investigation of Innovative Internal Trailing Edge Cooling Configurations with Pentagonal Arrangement and Elliptic Pin Fin,” *Int. J. Rotating Mach.*, **2008**(2008), p. 109120 (10 pages).
- [17] Uzol O., and Camci C., 2005, “Heat transfer, pressure loss and flow field measurements downstream of staggered two-row circular and elliptical pin fin arrays,” *J. Heat Transf.*, **127**(5), pp. 458–71.
- [18] Ames F. E., Nordquist C. A., and Klennert L. A., 2007, “Endwall Heat Transfer Measurements in a Staggered Pin Fin Array with an Adiabatic Pin,” 2007 ASME Turbo Expo, May 14, 2007 - May 17, 2007, American Society of Mechanical Engineers, pp. 423–432.
- [19] Ames F. E., and Dvorak L. A., 2006, “The Influence of Reynolds Number and Row Position on Surface Pressure Distributions in Staggered Pin Fin Arrays,” 2006 ASME 51st Turbo Expo, May 6, 2006 - May 11, 2006, American Society of Mechanical Engineers, pp. 149–159.
- [20] Ames F. E., Dvorak L. A., and Morrow M. J., 2005, “Turbulent Augmentation of Internal Convection over Pins in Staggered Pin Fin Arrays,” *Trans. ASME J. Turbomach.*, **127**(1), pp. 183–90.
- [21] Ostanek J. K., and Thole K. A., 2012, “Flowfield Measurements in a Single Row of Low Aspect Ratio Pin Fins,” *J. Turbomach.*, **134**(5), p. 051034 (10 pp.).
- [22] Ostanek J. K., and Thole K. A., 2012, “Wake Development in Staggered Short Cylinder Arrays within a Channel,” *Exp. Fluids*, **53**(3), pp. 673–97.
- [23] Busche M. L., Moualeu L. P., Chowdhury N., Tang C., and Ames F. E., 2013, “Heat Transfer and Pressure Drop Measurements in High Solidity Pin Fin Cooling Arrays With Incremental Replenishment,” *J. Turbomach.*, **135**(4), pp. 041011–041011.
- [24] Ostanek J. K., and Thole K. A., “Effects of Varying Streamwise and Spanwise Spacing in Pin-Fin Arrays.”
- [25] Ostanek J. K., 2012, “Flowfield Interactions in Low Aspect Ratio Pin-Fin Arrays,” Doctor of Philosophy Dissertation, Penn State University.
- [26] Moffat R. J., 1988, “Describing the Uncertainties in Experimental Results,” *Exp. Therm. Fluid Sci.*, **1**(1), pp. 3–17.